

Yb fiber amplifier at 972.5 nm with frequency quadrupling to 243.1 nm

Z. Burkley¹ · C. Raser¹  · S. F. Cooper¹ · A. D. Brandt¹ · D. C. Yost¹

Received: 22 July 2016 / Accepted: 7 November 2016 / Published online: 15 December 2016
© Springer-Verlag Berlin Heidelberg 2016

Abstract We demonstrate a continuous-wave ytterbium-doped fiber amplifier which produces 6.3 W at a wavelength of 972.5 nm. We frequency-quadruple this source in two resonant doubling stages to generate 530 mW at 243.1 nm. Radiation at this wavelength is required to excite the 1S–2S transition in atomic hydrogen and could therefore find application in experimental studies of hydrogen and anti-hydrogen.

1 Introduction

The hydrogen 1S–2S two-photon transition was first observed by Hänsch et al. [1]. Over the following four decades, the continued improvement in the spectroscopy of this transition has led to increasingly precise determinations of the Rydberg constant and proton charge radius—ultimately providing a stringent test of quantum electrodynamics [2]. The importance of the 1S–2S transition stems in part from the simplicity of hydrogen, which makes it amenable to theoretical study, and also from its narrow natural linewidth of only 1.3 Hz.

When reviewing the well-known measurements of the 1S–2S transition, one can also observe a continual refinement of the spectroscopy lasers used—first, by a transition from pulsed to continuous-wave (cw) lasers [3, 4] and then by an increase in power, coherence and robustness

[5–9]. The most recent result was reported by the Hänsch group in 2011, in which they determined the transition to a fractional frequency uncertainty of 4.2×10^{-15} [10]. By that time, the UV laser source had evolved to an all solid state system that produced 13 mW of 243 nm cw radiation. This radiation was then cavity enhanced to 368 mW within the hydrogen spectrometer. In addition to the impressive intracavity power, this radiation source possessed an extremely narrow linewidth of ≈ 1 Hz which is commensurate with the hydrogen 1S–2S transition width itself. More recently, in 2013, Beyer et al. [11] reported on a 243 nm laser which was capable of producing 75 mW before cavity enhancement.

Notwithstanding these accomplishments, we believe that continuing to increase the laser power at 243 nm would be very beneficial. For instance, the 1S–2S transition could be excited with laser beams of large transverse dimensions, which could decrease transit-time broadening and increase the proportion of atoms in the atomic beam that are excited. With the recent trapping of anti-hydrogen in its ground state, a larger beam would also prove beneficial in mitigating the difficulties created by the low number of trapped anti-hydrogen atoms available [12, 13]. However, we are mainly motivated to develop a power-scalable 243 nm laser in order to explore proposals to laser cool atomic hydrogen using the 1S–2S transition [14–16].

Spectroscopy of hydrogen and the recently trapped anti-hydrogen would benefit tremendously from robust laser cooling. Two-photon laser cooling could be more rapid and flexible than the more traditional approach using Lyman-alpha radiation at 121.6 nm—mostly due to the greater ease of producing radiation at 243 nm. To obtain reasonable scattering rates with such schemes requires that the 2S state be coupled to a state with short lifetime—for instance either the 2P [15] or 3P [16] states—and the average power

This article is part of the topical collection “Enlightening the World with the Laser” - Honoring T. W. Hänsch guest edited by Tilman Esslinger, Nathalie Picqué, and Thomas Udem.

✉ Z. Burkley
zakary.burkley@colostate.edu

¹ Colorado State University, Fort Collins, CO 80523, USA

of the cavity enhanced 243 nm radiation source should be at the ~ 100 W level. For a beam diameter of $500 \mu\text{m}$, this would lead to a scattering rate of ~ 500 Hz when maximally coupling the 2S and 2P states [15]. Power enhancement within an optical cavity can reach factors of ~ 100 with commercially available mirrors so that Watt-level 243 nm sources could be sufficient for an initial demonstration of cooling.

Here, we present a laser system that is a major step toward laser cooling hydrogen with the two-photon 1S–2S transition. The system is composed of an extended cavity laser diode (ECDL) at 972 nm followed by a tapered amplifier (TA), a ytterbium-doped double-clad fiber amplifier, and two consecutive resonant doubling stages. The ytterbium (Yb) fiber amplifier is a notable feature of this source since gain is much more readily obtained in Yb systems near 1030 nm due to the low absorption cross section at this wavelength. Gain near the emission cross-sectional peak at 976 nm is also possible but requires population inversions near 50% because the absorption cross section in that spectral region has approximately the same magnitude. Despite this difficulty, there have been demonstrations of 100 W Yb-doped fiber lasers near the emission cross-sectional peak at 976 nm [17, 18]. These lasers, however, operated at or above 976 nm. Below 976 nm, the emission cross section drops rapidly and the inversion required to obtain gain is $>50\%$. For our Yb-doped fiber, the emission cross section at 972 nm is approximately one-half the peak value. To the best of our knowledge, there have been only a few Yb fiber-based laser systems which operate at wavelengths shorter than 976 nm and these produced relatively low power (~ 10 mW) [19, 20]. The Yb fiber amplifier we demonstrate here outputs 6.3 W of power at 972 nm which upon frequency quadrupling yields 530 mW of power at 243 nm. We believe this approach is power scalable and that we can continue to increase our UV radiation with additional power at 972 nm.

2 Seed laser and Yb fiber amplifier

The master oscillator is an ECDL with an extended 10-cm-long cavity. This relatively long cavity length was chosen to increase the coherence of the oscillator [9]. The ECDL produces 30 mW of power at 972 nm and the design is shown in Fig. 1. The output of the oscillator is amplified to 3 W with a commercial tapered amplifier (DILAS). The manufacturer specified M^2 of the TA is only <1.7 , and we have measured ≈ 2.4 W within a TEM_{00} mode at the full power of 3 W. The output from the TA is then further amplified within a double-clad Yb-doped fiber (CorActive) with a $20 \mu\text{m}$ diameter core and $128 \mu\text{m}$ cladding. The core of this fiber has a numerical aperture of 0.075 which is large

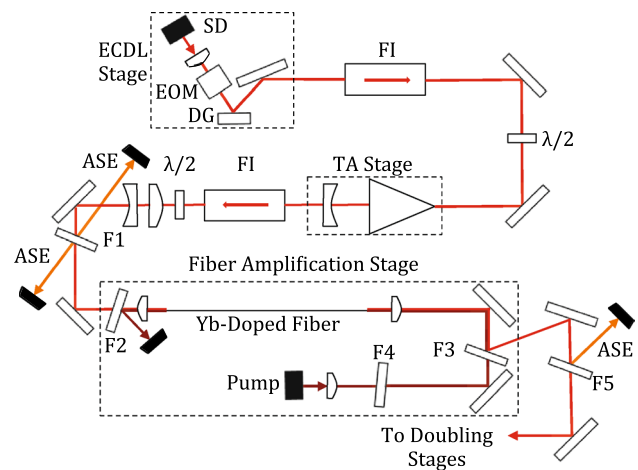


Fig. 1 Schematic of the ECDL master oscillator and amplification stages. SD: Seed diode, DG: diffraction grating, FI: Faraday isolator, F1 and F5: bandpass filters, F2: longpass filter, F3 and F4: shortpass filters. The ECDL contains an electro-optic modulator (EOM) for fast frequency control although it was not used for the studies here

enough to support the propagation of a few higher-order modes. However, we have observed the majority of the TA output power not contained within the TEM_{00} mode exists in transverse modes of significantly higher order. These modes cannot propagate through the fiber; thus, the fiber acts as a spatial filter.

The population inversion necessary to obtain gain at 972 nm requires that a high pump intensity at 915 nm be maintained along the entire length of the fiber, which results in low pump absorption. In our case, we use a short section of fiber (≈ 10 cm) that absorbs only 0.6 dB of the incident pump power. Due to the high population inversion within the fiber amplifier, there is also significant gain within the 1015 and 976 nm spectral regions. This is problematic as significant amplified spontaneous emission (ASE) would degrade the amplifier performance by reducing the population inversion. As shown in [21], the gain at a given wavelength within a homogeneously broadened amplifier can be written as a function of the gain or absorption at two other wavelengths and their respective absorption and emission cross sections. Using the cross-sectional data for our fiber [22], we find an expression for the gain (G_λ) at 976 nm given by

$$G_{976} = 2.41 \cdot G_{972} + 1.08 \cdot \beta A_{915}. \quad (1)$$

Here A_{915} is the absorption of the pump at 915 nm, and β is the ratio of the cladding area to the core area. In our amplifier, $\beta \approx 41$ and $A_{915} \approx 0.6$ dB. With a gain of $G_{972} \approx 4$ dB (given by our experimental results), the gain at 976 nm is $G_{976} \approx 37$ dB. Similarly, the gain at 1015 nm where there is also a peak in the emission cross section of our fiber is given by

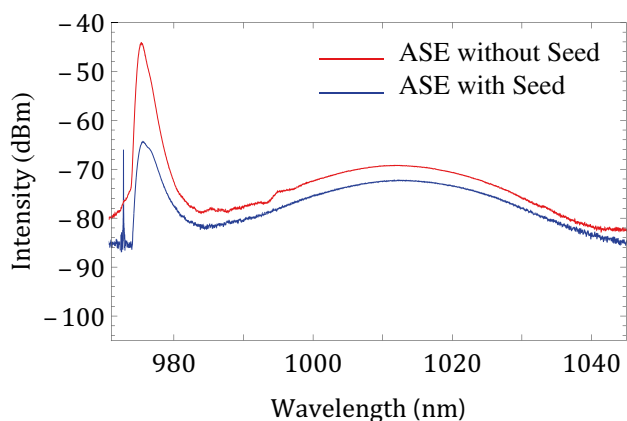


Fig. 2 Backward propagating radiation from the Yb fiber amplifier with and without seed. Both spectra were taken with 22.5 W of pump power at 915 nm

$$G_{1015} = 0.70 \cdot G_{972} + 1.64 \cdot \beta A_{915}, \tag{2}$$

which results in $G_{1015} \approx 43$ dB. As can be seen from the previous expressions, the gain at 976 and 1015 nm depends sensitively on the pump absorption due to the large value of β . As discussed extensively in [17, 18, 21], increasing the pump absorption, and therefore efficiency of the amplifier, would need to be accompanied by a decrease in β to keep the gain near 976 and 1015 nm manageable. Even in our current configuration, the large gain at 976 and 1015 nm would cause the amplifier to lase if the ends of the gain fiber were flat cleaved. To mitigate these effects, we angle-polish the ends of the gain fiber and use bandpass filters (FWHM = 4 nm) to reduce ASE originating from both the fiber amplifier and the TA [20]. The high inversion in the fiber can also lead to photodarkening—a poorly understood decrease in the optical transmission of gain fibers which degrades performance [23]. Mitigation of this effect is possible by codoping the gain fiber with phosphorous or cerium [24, 25]. We use a fiber codoped with phosphorous because it was commercially available; we have yet to observe any such degradation of the amplifier performance due to this effect.

Figure 2 shows the backward propagating radiation from the Yb fiber amplifier when pumping with 22.5 W of 915 nm radiation. Without seed power, the high inversion favors gain at 976 nm. With seed power, the peak at 976 nm is still dominant; however, this is due to ASE from the TA which is incompletely attenuated by filter F1 in Fig. 1. Back reflections from the output facet of the amplifier fiber also cause this radiation to be amplified in the reverse direction, along with a small amount of the 972 nm radiation. Without seed, the integrated power in Fig. 2 is \approx

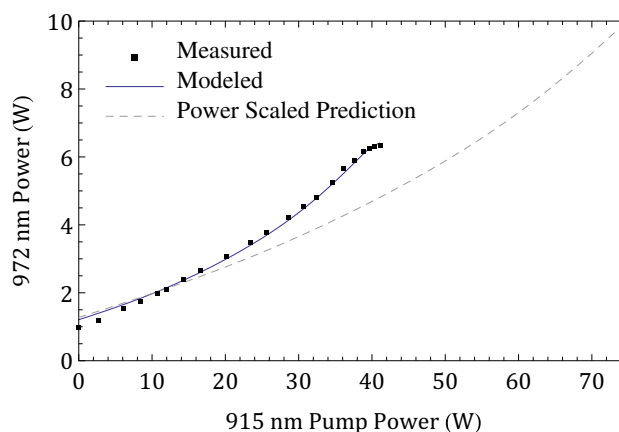


Fig. 3 Measured radiation at the output of the fiber amplifier as a function of 915 nm pump power. A linear fit to our data indicates a slope efficiency of $\approx 13\%$. The measured values agree well with a theoretical model (solid line) based on [18]. The nonlinear behavior is due to an increase in the pump wavelength as the diode current is increased. This effect is more pronounced in our system due to the low absorption of the pump power. Our model predicts that more power at 972 nm could be obtained with a pump diode that provides 130 W of output power (dashed line) and reaches the 915 nm absorption peak at a higher power [26]

270 mW, but this drops to only ≈ 9 mW when seeded. The ASE is roughly linear with pump power and therefore does not significantly degrade the amplifier performance for this short length of fiber.

The 972 nm output power of the fiber amplifier as a function of 915 nm pump power is shown in Fig. 3. Amplification of the 2.4 W of seed occurs at ≈ 15 W of pump power. However, even with zero pump power, significant inversion of the gain medium can occur due only to the input seed radiation, so that the fiber exhibits semi-transparency before the amplification threshold. At our maximum pump power of 41.5 W, we obtain an output power of 6.3 W at 972 nm, corresponding to a gain of 4.2 dB. The roll-off at high pump power is a result of the pump wavelength shifting away from the absorption peak at 915 nm as the diode current is increased. This effect is more pronounced in our system due to the low absorption of the pump. If the pump radiation did not shift with diode current, our models indicate there would be a near linear increase in the output power as a function of pump power.

Unfortunately, several common techniques to increase the efficiency of fiber amplifiers are not possible for our system. For example, an increase in fiber length without a decrease in β will result in unmanageable gain at 976 and 1015 nm. A double pass pump configuration is also not possible as the low single pass absorption of the Yb fiber amplifier could damage our pump diode. More specific

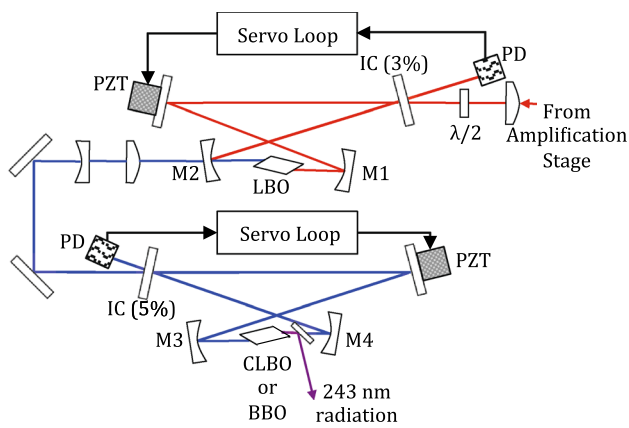


Fig. 4 Experimental setup of doubling stages. PD: Photodiode, PZT: piezoelectric transducer, IC: input coupler, M1–M4: 200 mm ROC mirrors. Since the optimal input coupler transmission depends on the power of the fundamental [28], we use input couplers with higher transmission than optimal to increase robustness and allow for power scaling

techniques such as ring-doping [21] and ultra large-mode-area rod-type photonic crystal fibers [17, 18] enabled Yb-doped fiber amplifiers with $\approx 60\%$ efficiency between 976 and 980 nm. To our knowledge, the former is not commercially available. The latter, although commercially available, have no long-term studies testing their resilience against photodarkening at high inversion. In addition, their length cannot be changed once constructed. One potentially interesting avenue would be Yb-doped fiber with smaller cladding/core ratio (β), which is also codoped with phosphorous to prevent photodarkening.

Despite the low efficiency of this amplifier, the outlook for scaling the power, which is the primary concern for laser cooling atomic hydrogen, seems promising. Modeling the performance of our amplifier using the method found in [18], we can theoretically reproduce the measured performance. As shown in Fig. 3, the model also indicates that we can continue to increase the output power with a pump diode that reaches 915 nm at higher power [26]. The same model suggests an additional amplification stage could also be an effective means to increase the output power [27].

3 Doubling stages

As shown in Fig. 4, the output of the fiber amplifier is frequency-quadrupled to 243 nm in two consecutive resonant doubling stages. The first stage uses lithium triborate (LBO) as the nonlinear crystal (United Crystals), while for the second we tested both beta barium borate (BBO) and cesium lithium triborate (CLBO) as the nonlinear crystals (Crystals of Siberia and Altechna, respectively).

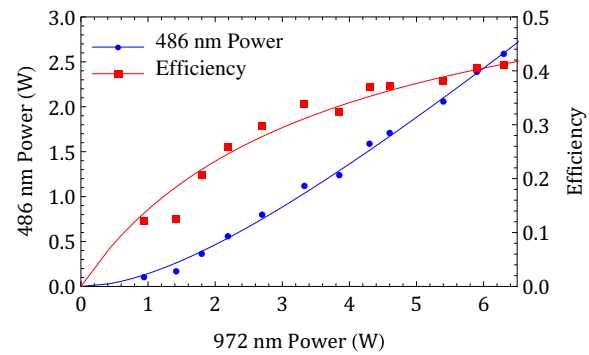


Fig. 5 Experimental results of frequency doubling fiber amplified 972 nm radiation using LBO as the nonlinear medium. With 6.3 W of power at 972 nm, up to 2.60 W of power at 486 nm is generated. The solid lines follow the model in [28, 30]

The first nonlinear doubling stage uses a standard bow-tie geometry. The curved mirrors have a radius of curvature (ROC) of 200 mm, producing a $62 \mu\text{m}$ beam waist within the 25-mm-long LBO crystal. This mode size, which is ≈ 1.8 times the optimal waist determined from the Boyd–Kleinman focusing criteria [29], increases the robustness of the doubling stage with minimal effect on the overall conversion efficiency. We use type I non-critical phase matching in order to eliminate spatial walk-off and improve the 486 nm output beam quality, which requires the LBO be kept at a temperature of $283 \text{ }^\circ\text{C}$. Alternatively, walk-off could be eliminated with the use of periodically poled nonlinear materials. However, one of our primary concerns for this work is robustness and high damage threshold, and we believe periodically poled nonlinear crystals are less proved in this regard. The first stage uses an input coupler with a transmission of 3%, which is larger than the theoretical optimal ($T_{opt} \approx 2\%$ at the highest fundamental power) [28]. This allows for power scaling since the optimal input coupler transmission will increase with additional fundamental power.

Because the performance of typical dual wavelength anti-reflection coatings is not guaranteed at high temperatures, we use a Brewster-cut crystal to reduce the loss of the resonant 972 nm light. This leads to an 18% loss of the generated 486 nm radiation from the Fresnel reflection on the crystal output facet. The remaining 82% of the 486 radiation is coupled out of the cavity through a dichroic curved mirror with high reflectivity at 972 nm and high transmission ($>90\%$) at 486 nm. The 486 nm output power as a function of incident fundamental power is shown in Fig. 5. We obtain 2.4 W of 486 nm radiation with 6.3 W of 972 nm fundamental power. The theoretical fit for harmonic conversion used in Fig. 5 follows the model presented in [28, 30]. The data can be fit reasonably well with

a range of parameters in which the transverse mode matching is greater than 80% and the roundtrip linear losses are less than 1.2%.

To stabilize the doubling cavity to the fundamental radiation, we modulate one cavity mirror at a frequency of ≈ 300 kHz and detect the modulated cavity power with a photodiode (see Fig. 4). We then demodulate this signal with a double-balanced mixer to generate an error signal, which is sent to a loop filter followed by a fast (~ 50 kHz bandwidth) piezoelectric transducer and a slow (~ 100 Hz) transducer with greater range. A nearly identical setup is used to maintain the resonance condition within the second doubling stage.

In the second doubling stage, which produces 243 nm radiation, we tested both a BBO crystal and a CLBO crystal [31–34] in type I critical phase matching configurations. CLBO has a lower nonlinear coefficient than BBO, but also less spatial walk-off and a higher damage threshold [35]. Similar to the first stage, the second doubling stage is a bow tie design with 200 mm ROC mirrors to produce a focus in the nonlinear crystal. This produces a beam waist of $44 \mu\text{m}$ that is ≈ 1.9 times the Boyd–Kleinman focusing criteria [29] in order to prevent damage of the nonlinear crystal at high intensities and to minimize walk-off effects. The input coupler for this cavity was 5% to increase robustness and allow for power scaling. Both crystals are Brewster cut and 10 mm long. In this case, Brewster-cut crystals are used because AR coatings are not yet well developed for CLBO crystals [32]. This introduces a 27% output coupling loss for the 243 nm light with the BBO crystal, and an 18% loss with the CLBO crystal due to the Fresnel reflection on the output facet of the crystal. The BBO crystal is cut at $\theta = 55^\circ$ and has a double refraction angle of $\rho = 82$ mrad. For CLBO, $\rho = 18$ mrad and the crystal is cut at $\theta = 77^\circ$. As shown in Fig. 4, a Brewster oriented dichroic mirror with high reflectivity at 243 nm and high transmission at 486 nm is used to output couple the 243 nm radiation.

The observed 243 nm output power as a function of the 486 nm input power is shown in Fig. 6 when using the BBO crystal and in Fig. 7 for the CLBO crystal. The theoretical curves again follow the model presented in [28, 30], and assume a 2% roundtrip linear loss along with 80% transverse mode matching. As can be seen from the figures, a greater efficiency was obtained with the CLBO crystal due to the smaller walk-off and smaller Fresnel loss from the Brewster-cut crystal. This also produces a 243 nm beam with less ellipticity, which will be easier to shape and couple into a 243 nm enhancement cavity.

Due to the high UV power generated, crystal degradation is a concern. Frequency doubling studies at a similar wavelength have demonstrated 5 W of 266 nm power without damaging the CLBO crystal [32]. This corresponds to

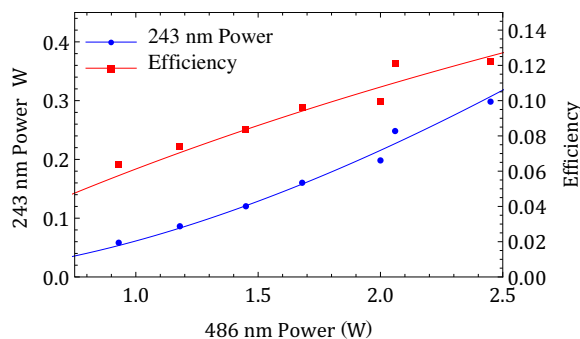


Fig. 6 Experimental results of frequency doubling 486 nm radiation to 243 nm radiation using BBO as the nonlinear medium. With 2.45 W of 486 nm radiation, up to 300 mW of power at 243 nm is generated. The solid lines follow the model in [28, 30]

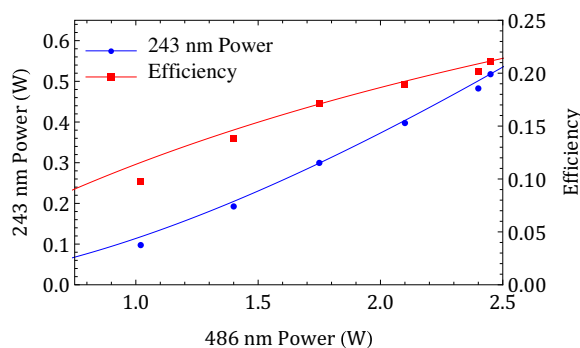


Fig. 7 Experimental results of frequency doubling 486 nm radiation to 243 nm radiation using CLBO as the nonlinear medium. With 2.45 W of 486 nm radiation, up to 530 mW of power at 243 nm is generated. The solid lines follow the model in [28, 30]

≈ 5 times greater UV intensity within the crystal compared to the results reported here. Additional studies have shown that if degradation in CLBO occurs, it appears to be reversible [36]. This is in contrast to BBO, which shows irreversible damage caused by the formation of absorption centers [31, 36, 37]. Therefore, by utilizing CLBO we should be able to power scale our UV output as more fundamental power becomes available without crystal degradation.

CLBO is also known to be hygroscopic and some performance change has been reported as the crystal absorbs or desorbs water [38]. For this reason, the CLBO crystal is operated at a temperature of 130°C . Over a few days at this elevated temperature, the conversion efficiency increased slightly above that shown in Fig. 7 and we observed >530 mW of 243 nm radiation over 50 min with no degradation.

4 Conclusion

We have demonstrated a fiber-based amplifier laser system capable of generating 6.3 W of power at 972 nm. Upon frequency doubling in successive resonant cavities, this laser source can generate 2.4 W at 486 nm and 530 mW at 243 nm. We are encouraged by the power scalability of our system. Simulations indicate that our fiber amplifier platform should be able to produce additional 972 nm radiation either with more powerful, commercially available pump diodes or with an additional fiber amplifier stage of similar design [27]. To use the 915 nm pump radiation more efficiently would require that we obtain fibers with a smaller cladding/core area ratio (β), such as the rod-type fibers used in [17, 18], with the addition of phosphorous codoping to increase resilience against photodarkening. The doubling stages were designed with relatively loose focusing in the crystals and high transmission input couplers. This, in conjunction with the high damage thresholds of LBO and CLBO, make us hopeful that these cavities can also be power scaled.

Although we made no in-depth studies of the linewidth of our laser source for the work described here, our seed laser copies many aspects of the low phase noise design described in [9] and we were able to couple our radiation into doubling cavities with few MHz resonance widths without any difficulty. For two-photon laser cooling of hydrogen, the transition width will be broadened to ≈ 50 MHz by coupling the 2S and 2P states. Therefore, the laser source we describe here already has the coherence necessary for that application. That being said, spectroscopy of the hydrogen and anti-hydrogen 1S–2S transition with a power scaled 243 nm system would be very beneficial but would also require the source possess an extremely narrow linewidth. Stabilizing the frequency of this source to that level will therefore be the subject of future work.

Acknowledgements We gratefully acknowledge Jacob Roberts for useful discussions and for carefully reviewing this manuscript.

References

1. T.W. Hänsch, S.A. Lee, R. Wallenstein, C. Wieman, *Phys. Rev. Lett.* **34**, 307 (1975)
2. P.J. Mohr, B.N. Taylor, D.B. Newell, *Rev. Mod. Phys.* **84**, 1527 (2012)
3. B. Couillaud, T. Hänsch, S. MacLean, *Opt. Commun.* **50**, 127 (1984)
4. C.J. Foot, B. Couillaud, R.G. Beausoleil, T.W. Hänsch, *Phys. Rev. Lett.* **54**, 1913 (1985)
5. M.G. Boshier et al., *Phys. Rev. A* **40**, 6169 (1989)
6. R. Kallenbach, F. Schmidt-Kaler, M. Weitz, C. Zimmermann, T.W. Hänsch, *Opt. Commun.* **81**, 63 (1991)
7. C. Zimmermann, V. Vuletic, A. Hemmerich, T.W. Hänsch, *Appl. Phys. Lett.* **66**, 2318 (1995)
8. N. Kolachevsky, J. Alnis, S.D. Bergeson, T.W. Hänsch, *Phys. Rev. A. (Rapid Communications)* **73**(021801(R)) (2006)
9. N. Kolachevsky, J. Alnis, C. Parthey, A. Matveev, R. Landig, T. Hänsch, *Opt. Lett.* **36**, 4299 (2011)
10. C. Parthey, A. Matveev, J. Alnis, B. Bernhardt, A. Beyer, R. Holzwarth, A. Mastrou, R. Pohl, K. Predehl, T. Udem, T. Wilken, N. Kolachevsky, M. Abgrall, D. Rovera, C. Salomon, P. Laurent, T. Hänsch, *Phys. Rev. Lett.* **107**, 203001 (2011)
11. A. Beyer, J. Alnis, K. Khabarova, A. Matveev, C. Parthey, D. Yost, R. Pohl, T. Udem, T. Hänsch, N. Kolachevsky, *Ann. Phys. (Berlin)* **525**, 671 (2013)
12. G. Gabrielse, R. Kalra, W.S. Kolthammer, R. McConnell, P. Richerme, D. Grzonka, W. Oelert, T. Seifzick, M. Zielinski, D.W. Fitzakerley, M.C. George, E.A. Hessels, C.H. Story, M. Weel, A. Müllers, J. Walz, *Phys. Rev. Lett.* **108**, 113002 (2012)
13. G. Andersen et al., *Nat. Phys.* **7**, 558 (2011)
14. V. Zehl, J.C. Garreau, *Phys. Rev. A. (Rapid Communications)* **63**, 021402(R) (2001)
15. D. Kielpinski, *Phys. Rev. A* **73**, 063407 (2006)
16. S. Wu, R. Brown, W. Phillips, J. Porto, *Phys. Rev. Lett.* **106**, 213001 (2011)
17. J. Bouillet, Y. Zaouter, R. Desmarchelier, M. Cazaux, F. Salin, J. Saby, R. Bello-Doua, E. Cormier, *Opt. Express* **16**, 17891 (2008)
18. F. Röser, C. Jauregui, J. Limpert, A. Tünnermann, *Opt. Express* **16**, 17310 (2008)
19. D. Hanna, R. Percival, I. Perry, R. Smart, P. Suni, A. Tropper, *J. Mod. Opt.* **37**, 517 (1990)
20. J. Yi, Y. Fan, S. Huang, *IEEE Photonics J.* **4**, 2278 (2012)
21. J. Nilsson, J. Minelly, R. Paschotta, A. Tropper, D. Hanna, *Opt. Lett.* **23**, 355 (1998)
22. Fiber data given to authors from CorActive upon author's request
23. J. Koponen, M. Söderlund, H. Hoffman, *Opt. Express* **14**, 11539 (2006)
24. M. Engholm, L. Norin, *Opt. Express* **16**, 1260 (2008)
25. M. Engholm, P. Jelger, F. Laurell, L. Norin, *Opt. Lett.* **34**, 1285–1287 (2009)
26. nLIGHT Photonics – model: e12.1300915105
27. D. Richardson, J. Nilsson, W. Clarkson, *J. Opt. Soc. Am. B* **27**, 63 (2010)
28. E. Polzik, H. Kimble, *Opt. Lett.* **16**, 1400 (1991)
29. G. Boyd, D. Kleinman, *J. App. Phys.* **39**, 3597 (1968)
30. R. Targat, J. Zondy, P. Lemonde, *Opt. Commun.* **247**, 471 (2005)
31. M. Scheid, F. Markert, J. Walz, J. Wang, M. Kirchner, T. Hänsch, *Opt. Lett.* **32**, 955 (2007)
32. J. Sakuma, Y. Asakawa, T. Sumiyoshi, H. Sekita, *IEEE J. Sel. Top. Quantum Electron.* **10**, 1244 (2004)
33. J. Hu, L. Zhang, H. Liu, K. Liu, Z. Xu, Y. Feng, *Opt. Express* **21**, 30958 (2013)
34. Y. Kaneda, J. Yarborough, L. Li, N. Peyghambarian, L. Fan, C. Hessenius, M. Fallahi, J. Hader, J. Moloney, Y. Honda, M. Nishioka, Y. Shimizu, K. Miyazono, H. Shimatani, M. Yoshimura, Y. Mori, Y. Kitaoka, T. Sasaki, *Opt. Lett.* **33**, 1705 (2008)
35. Y. Mori, I. Kuroda, S. Nakajima, T. Sasaki, S. Nakai, *Jpn. J. Appl. Phys.* **34**, 296 (1995)
36. K. Takachiho, M. Yoshimura, Y. Takahashi, M. Imade, T. Sasaki, Y. Mori, *Opt. Mat. Exp.* **4**, 559 (2014)
37. K. Kondo, M. Oka, H. Wada, T. Fukui, N. Umezu, K. Tatsuki, S. Kubota, *Opt. Lett.* **23**, 195 (1998)
38. T. Kawamura, M. Yoshimura, Y. Honda, M. Nishioka, Y. Shimizu, Y. Kitaoka, Y. Mori, T. Sasaki, *App. Opt.* **48**, 1658 (2008)